A NOVEL ENERGY CONVERSION SYSTEM BASED ON SUPERCRITICAL CO_2 RECOMPRESSION BRAYTON POWER CYCLE FOR POWER TOWER CONCENTRATING SOLAR PLANTS

José I. Linares[1], María J. Montes[2], Alexis Cantizano[1], Consuelo Sánchez[2]

[1] Comillas Pontifical University, Alberto Aguilera, 25, 28015 Madrid, Spain

[2] Universidad Nacional de Educación a Distancia (UNED), Juan del Rosal 12, 28040 Madrid, Spain

ABSTRACT

Power tower concentrating solar plants with thermal energy storage are called to play a key role in the future energy transition to a low carbon scenario, thanks to be a dispatchable renewable energy. The goals proposed for the new power plants, so in cost reduction as in high temperatures conditions, lead to technological challenges, which should be overcome.

The ternary $MgCl_2$/KCl/NaCl salt appears as one of the most promising heat transfer fluid due to its lower melting point, higher heat capacity, lower cost and stability up to 800 °C. A cavity-type receiver has been selected as the most suitable design to minimize radiation heat loss at high working temperatures, compared to an external-type receiver, since there are no commercial selective coatings that do not degrade in air. Supercritical Brayton power cycle is the selected technology for the power block because of its potential to surpass 50 % efficiency even working in dry cooling conditions. Printed circuit heat exchangers are recommended for this type of Brayton cycle due to its ability to support the high pressures usually found. However, plugging and clogging issues arise from the use of molten salts in the small channels of these heat exchangers.

This paper proposes a novel supercritical CO_2 Bayton power cycle whose heat power is supplied through the low pressure side (over 85 bar), so allowing the use of shell and tube heat exchangers for molten salt/CO_2 heat transfer process. Different options based on the recompression layout with intercooling and reheating have been investigated in both dry and wet cooling scenarios. Reheating option is recommended for wet cooling, reaching 54.6 % efficiency and investment of 9,296 $/kWe; intercooling with reheating is the best option for dry cooling, reaching 52.6 % efficiency and investment of 9,381 $/kWe.

[1] linares@comillas.edu

ACRONYMS

AC	Auxiliary Compressor
ASME	American Society of Mechanical Engineers
CP	Cooling pump
CSP	Concentrating Solar Plants
FCI	Fixed Capital Investment
HPT	High Pressure Turbine
HTF	Heat Transfer Fluid
HTP	High Temperature Pump (in the heating loop)
HTR	High Temperature Recuperator
IC	Intercooling, intercooler
LP	Low Pressure heat power feeding
LPT	Low Pressure Turbine
LTP	Low Temperature Pump (in the heating loop)
LTR	Low Temperature Recuperator
M	Magnitude for scaling costs
MC	Main Compressor
MC1	Low Pressure Main Compressor
MC2	High Pressure Main Compressor
MCIT	Main Compressor Inlet Temperature
MS	Molten Salt
NREL	National Renewable Energies Laboratory
OFFSC	Off-site Costs
ONSC	On-site Costs
p	Pressure
PC	Pre-cooler
PCHE	Printed Circuit Heat Exchanger
PEC	Purchased-Equipment Costs
PTS	Power Tower Solar
RC	S-CO2 Recompression layout
RH	Reheating, reheater
S-CO2	Supercritical Brayton Power Cycle
SHX	Source Heat Exchanger
SHXIT	CO_2 inlet temperature to the Source Heat Exchanger
SNL	Sandia National Laboratory
STHE	Shell and Tubes Heat Exchanger
T	Temperature, Turbine
TEMA	Tubular Exchanger Manufacturers Association
TES	Thermal Energy Storage
TIP	Turbine Inlet Pressure
W	Power

NOTATION

Latin letters

a	Escalation factor
c	Specific heat
C	Cost
CI	Cost index
D	Diameter
f	Factor
h	Height
M	Generic Magnitude
$\dot{W}$	Power

Greek Letters

η	Efficiency
ρ	Density

Subscripts

0	Basis case
0y	Basis reference year
A	Heat transfer area
AC	Auxiliary Compressor
b	Baseline heat exchanger cost
CP	Cooling pump
cycle	Cycle
E	Cost refereed to 1982
ERy	Cost corrected to the reference year "y"
f	Cost multiplier in shell and tube cost estimation
g	Generator
gross	Gross
HPT	High Pressure Turbine
HTP	High Temperature Pump (in the heating loop)
i	Correcting factors in shell and tube cost estimation
LPT	Low Pressure Turbine
LTP	Low Temperature Pump (in the heating loop)
MC	Main Compressor
MC1	Low Pressure Main Compressor
MC2	High Pressure Main Compressor
net	Net
p	Pressure; Cost multiplier in shell and tube cost estimation
r	Cost multiplier in shell and tube cost estimation
Ry	Reference year "y"
sh	Shell
T	Turbine
T	Temperature
t	Tower
TMG	Turbomachines and Generator
tower	Tower
W	Power

1. INTRODUCTION

The progressive replacement of fossil power plants with clean energies is one of the challenges facing humanity today. Among the clean energies, the renewable ones have an important role, especially due to their local origin. However, the most currently developed renewable energies (solar PV and wind) have the penalty of the intermittence, which leads to fossil back-up systems. One way forward to tackle this issue is the use of energy storage systems in the power plants, being one of the most promising technologies the thermal solar energy storage (TES) used in the concentrated solar power (CSP) plants. These plants face to several challenges, including the currently high generation costs, but the advantage of the TES converses them into one promising alternative in a future energy scenario that avoids global warming. So, the Solar Power Gen3 Demonstration Roadmap from the National Renewable Energies Laboratory (NREL) [Mehos-2017] has focused on power tower solar (PTS) systems with three pathways of TES: molten salts, falling particle and gas phase, establishing cost goals. For all the alternative pathways, the Roadmap states the supercritical CO_2 Brayton power cycle (S-CO2). NREL proposed a demonstration facility of 10 MWe with a cost over $200 million, although with uncertainty around this value. The receiver should work at high temperature (above 700 °C), which leads to replace the typical solar salt by other able to maintain stable at such temperatures. Regarding the power cycle, the goal is reaching efficiencies higher than 50 %. Similar goals are proposed in other research programmes, as in the Australian Solar Thermal Research Initiative (ASTRI) [ASTRI] or in the project developed by EDF in collaboration with Zhejiang University to design a 100 MWe plant with S-CO2 and molten salt (MS) as TES with power tower technology [Zhang-2018].

As conventional solar salts (nitrate salts) cannot be used above 600 °C, it is necessary to replace them by others in order to meet the target temperature of 700 °C or higher. Myers and Goswami [Myers-2016] show a review of chloride salts and their eutectics, which might be used for sensible or even latent TES. Li et al. [Li-2017] give equations for thermophysical properties of both binary and ternary eutectic salts from NaCl, KCl, $MgCl_2$, $CaCl_2$ and $ZnCl_2$ able to be used up to 800 °C. They recommend these salts as heat transfer fluid (HTF) to be used in CSP. Mohan et al. [Mohan-2018] assess the thermophysical properties and cost of a novel ternary eutectic salt mixture composed of NaCl, KCl and $MgCl_2$ for high temperature sensible storage. This novel salt has a melting point of 387 °C and is stable up to 800 °C, which makes it suitable for advanced power tower technology with two tank storage based in 500/700 °C. Besides that, this salt has a 32% lower volumetric heat capacity ($\rho \cdot c$), compared to conventional salts, so the volume of the storage tanks is smaller, given that tank size is inversely proportional to $\rho \cdot c_p \cdot \Delta T$. At last, its cost (currency 2016) is 295 $/tonne, which makes it competitive with nitrate salts (over 1,000 $/tonne, [Mehos-2017]). According with these authors, this novel ternary salt is the most promising candidate for high temperature applications. Xu et al. [Xu-2018] show experimental data of properties for this novel salt.

The receiver configuration selected has been a tubular cavity-type. Although the current state-of-art configuration for MS receivers is the tubular external-type [Mehos-2017], recent research [Turchi-2019]

recommends the cavity design as a way of not penalizing thermal efficiency when working at high temperature, where radiation heat loss becomes important. Cavity receivers are generally expected to have lower radiation heat loss than external receivers, while it is not available commercially a selective coating for tubes that withstand high temperature and does not degrade in air. A north-facing heliostat field is associated to these cavity-receivers. For all the layouts analysed in this work, the solar multiple is equal to 1.5; this value is a compromise between the energy availability in the thermal storage and a suitable receiver dimensions, as cavity receivers require a larger absorber surface area than external ones [Ho, 2014].

The conventional Brayton cycle (using an ideal gas as working fluid) presents the advantage of a high compactness due to the low size of the turbomachinery and also a simpler layout than the steam Rankine cycle. However, it demands a high compression power, issue overcome with high turbine inlet temperatures, usually around 1,200 °C and higher [Saravanamuttoo]. To maintain high efficiency at lower temperatures the working fluid should be replaced. So, using Helium in a closed cycle efficiencies higher than 50 % can be reached in high temperature reactors foreseen in nuclear fission Generation IV [Herranz-2009]. However, helium demands temperatures around 850÷950 °C to reach high efficiencies. When temperature rounds 500 °C, as in sodium fast reactor (another design foreseen in Generation IV), Brayton cycles with helium reduce a lot their efficiency [Pérez-Pichel-2011]. It is in these cases when the use of supercritical CO_2 as working fluid allows reaching again high efficiencies [Pérez-Pichel-2012].

The first proposals of CO_2 Brayton power cycles come from Sulzer in 1950 [Sulzer-1950]. Nearly twenty years later, Angelino [Angelino-1968] analysed several layouts of transcritical cycles, that is, with the heat rejection pressure below the critical pressure, which leads to condensate in the heat rejection process. This application requires a low heat sink temperature due to the low critical temperature of the CO_2 (around 31 °C). At the same time, Feher [Feher-1968] proposed the so-called supercritical cycle, that is, all the cycle working above the supercritical pressure. Likely due to the lack of the required turbomachines in that age, the researchers did not pay attention to S-CO2 until 2004, when Dostal [Dostal-2004] retook the cycle as power conversion system for sodium fast reactor (nuclear fission Generation IV programme). The key aspect of the S-CO2 is the closeness of the compressor inlet conditions to the critical point. In such region (above the critical pressure, but not far, usually between 75 and 90 bar) the density of the CO_2 is high, thus reducing the compression power a lot, allowing the use of moderate turbine inlet temperatures. So, 500 °C is enough to pass 40 %, achieving higher efficiencies than supercritical steam Rankine for turbine inlet temperatures higher than 550 °C [Dostal-2004].

When moderate to high temperatures in the thermal source are available the S-CO2 employs recuperators, that is, heat exchangers which recover the thermal energy in the fluid leaving the turbine to pre-heat the fluid before it enters into the heat source. The closeness of part of the cycle to the critical point makes the

heat recovery process complex, which is overcome with different arrangements, being the so called recompression the most common [Dostal-2004]. Depending on the source and heat sinks temperatures, variations including intercooling and reheating are possible. So, Wang et al. [Wang-2017] conclude that intercooling increases the efficiency at high compressor inlet temperatures (when dry cooling is used) and that reheating should be always included in S-CO2 for CSP applications, although it trends to reduce the molten salt temperature difference, so increasing the salt inventory. Ma et al. [Ma-2017] also recommend intercooling when dry cooling is using. Similar results are obtained by Binotti et al. [Binotti-2017]. On the other hand, Pérez-Pichel [Pérez –Pichel-2012] does not recommend neither intercooling nor reheating for sodium fast reactor applications (turbine inlet temperature about 500 °C).

Regarding the use of S-CO2 in CSP, especially in power tower solar, the research is recent. So, Iverson and Conboy in 2013 [Iverson-2013] claimed that the publications and research works for nuclear applications (focused on Generation IV) have experienced a large development, including experimental work, whereas the analysis for CSP is lower, in comparison. Later, some authors have paid attention to other applications, as it can be seen in the review carried out by Ahn et al. [Ahn-2015]. Li et al. [Li-2017-2] reviewed nuclear, solar energy, geothermal, waste heat recovery and fuel cell, gathering a survey about experimental facilities around the world. Turchi et al. [Turchi-2013] focused on CSP, covering the dry cooling, intercooling and reheating. Milani et al. [Milani-2017] proposed a hybrid fossil/solar design based on recompression with intercooling and reheating as a contribution to the transition to a low-carbon industry. Most recently, Wang et al. [Wang-2018] developed a multi-objective optimisation to select the best layout, finding the recompression with intercooling as the winner when high compressor inlet temperature occurs (dry cooling scenarios).

The high compactness of S-CO2 power cycles has revealed as one of its most attractive features. So, Xu et al. [Xu-2019] highlight the good dynamic response of the heat exchangers and the small turbomachines, which leads to supply grid stability against dynamic changes. This good behaviour against fluctuations also was observed by Iverson et al. [Iverson-2013] with small scale experiments, and predicted by Ma et al [Ma-2011], who analysed a PTS in direct cycle.

Dostal [Dostal-2004] recommend printed circuit heat exchangers (PCHE) for S-CO2 power cycles. This type of heat exchangers usually uses small semi-circular channels (around 2 mm diameter) in a very compact arrangement, achieving temperature approaches of 2 °C, which leads to effectiveness as high as 98 %. They are manufactured with diffusion bonding technology, which allows them to support high pressures (up to 800 bar) [Le Pierres-2011]. They can be manufactured in SS 316, recommended for temperatures up to 500 °C, and in Inconel 617 for higher [Southall-2008]. Huang et al. [Huang-2019] gathering several correlations to describe flow and heat transfer mechanisms in PCHEs.

From the point of view of the integration of the CSP into the grid, the most important issue is the ability to store energy, so improving the dispatchability [Mehos-2017]. However, several authors have warned about certain issues about the use of molten salts in PCHEs. So, Moore et al. [Moore-2010] discuss different type of heat exchangers for PTS with molten salts, saying that PCHEs technology is unproven in many applications, and expressing doubts about maintenance and cleaning, highlighting that plugging caused by the salt can be a serious problem. In s similar way, Sabharwall et al. [Sabharwall-2014] point out the thawing/clogging as a criterion to select the type of heat exchanger to be used with molten salts, saying that PCHEs currently exhibits some issues. In order to overcome such concerns, some authors have studied a modified PCHE with airfoils fins in the salt side and the common channels in the CO_2 side. So, Lao et al. [Lao-2019] have analysed such solutions, concluding that a deterioration in the heat transfer mechanism is observed. Wang et al. [Wang-2019] carried out an experimental work using the airfoil fins. They establish that shell and tubes heat exchangers (STHE) are not suitable for pressures higher than 200 bar, values usually found at S-CO2. Another modification of PCHEs to avoid the salt issues is the replacement of the common channels in the salt side by a rectangular fins structure, resulting in a large pass section for the salt. Unfortunately, this solution only is valid again up to 200 bar, so introducing limitations in the performance of the S-CO2 cycle [Kruizenga-204] [Sabharwall-2014]. In spite of pressure limitations of the STHE, some authors advocate by them, as He et al. [He-2016], who carry out experimental investigations, or Qiu et al. [Qiu-2018] who propose a new design of STHE, although they perform the analysis with molten salt in the shell but oil in the tubes side. Finally, Zhang et al. [Zhang-2018] propose STHE for molten salt/CO_2 heat exchanger in a PTS with S-CO2 and PCHEs for the recuperators, but the maximum pressure of the cycle is 200 bar.

One way forward to use STHE in S-CO2 with pressures higher than 200 bar would be supply the heat power to the cycle at pressure lower than the maximum. This can be done in the so called split expansion cycle, where the heat power is supplied at intermediate pressure between two turbines, as in a reheating, and the heat transfer upstream the high pressure turbine comes from the recuperator, fed with the flow leaving the low pressure turbine [Wang-2017].

This paper proposes a novel S-CO2 cycle for power tower concentrating solar plants using a molten salt two tank system as thermal energy storage. These types of plants cannot use PCHEs for the molten salt/CO_2 heat exchanger due to thawing/clogging concerns, being the shell and tube heat exchangers, with the salt in the shell, the most mature solution. However, STHE cannot be used above 200 bar, which limits a lot the optimisation of the S-CO2 cycle. The novel proposal comes from a previous design by the authors for a direct S-CO2 cycle for a fusion reactor, where the heat power were supplied downstream the turbine, transferring it to the turbine inlet trough a recuperator [EFDA-2013]. In this way, a STHE can be used as molten salt/CO_2 heat exchanger, working the tubes at pressure lower than 200 bar with maximum pressure cycles up to 300 bar. The cycle is based on the recompression layout, but intercooling and reheating have

been considered too, all in both wet and cooling scenarios. A comparison of the selected layouts has been carried out with equivalent classical S-CO2 solutions in order to assess the efficiency reduction. Finally, an economic assessment has been done to obtain the investment of a 50 MWe plant with 3 hours of energy storage.

2. METHODOLOGY

2.1. Cycles layouts

The key of the novel energy conversion system proposed is the heat power supply through the low pressure side. This enables the possibility of replacing the printed circuit heat exchanger by a more mature shell and tubes heat exchanger, with the molten salt circulating along the shell, so avoiding the melting/clogging issues. Figure 1 shows a comparison between the conventional recompression cycle (RC) and the novel cycle fed at low pressure (RC-LP). It is observed that in the novel design the heat power is transferred into the upstream turbine flow by means of the high temperature recuperator (HTR). Both cycles are based on the recompression concept, that is, the use of two compressors (main compressor, MC, and auxiliary compressor, AC) to manage the main issue of the supercritical CO_2 close to the critical point, that is, the clearly different specific heat with the pressure. So, high pressure stream leaving the main compressor (6 in Figure 1a and 7 in 1b) exhibits a higher specific heat than the low pressure stream incoming to the low temperature recuperator (LTR) (3 in Figure 1a and 4 in 1b). These different values of the specific heat would lead to locate the minimum temperature approach in the cold stream inlet, with a large approach in the cold stream outlet, so reducing the recovering effect. The recompression cycle splits the recuperator into two units (LTR and HTR), using two compressors to use a lower mass flow rate in the stream with the higher specific heat. According with [LINARES EFDA] the optimal split of the mass flow rate (split ratio, that is, the mass flow rate crossing the auxiliary compressor divided by the mass flow rate crossing the hot stream of the LTR) is that which achieves the same temperature approach at both extremes of the LTR (balanced heat exchanger).

It is observed how the AC inlet stream is taken upstream the pre-cooler, so its outlet reaches a high temperature, similar to the cold stream leaving the LTR, so reducing the irreversibility in the mixing point (7-8-9 in Figure 1a and 8-9-10 in 1b). Finally, in the HTR the same mass flow rate is used in both streams, due to the higher temperature than in the LTR reduces the difference in the specific heats. In Figure 1a the molten salt (MS) to CO_2 heat exchanger would have to be a PCHE, able to support the high pressure difference between both fluids (usually 250 to 300 bar in the CO_2 versus 5 to 6 bar in the molten salt). However, in Figure 1b a STHE heat exchanger can be used due to the low pressure in the CO_2 side (between 75 to 85 bar).

The cycle rejects the heat power to the thermal sink through the pre-cooler (PC). Taking into account the site conditions in CSP technologies two types of thermal sinks have been considered: wet cooling, which leads to a CO_2 to water pre-cooler, and dry cooling using an air-cooled pre-cooler, typical solution in arid sites.

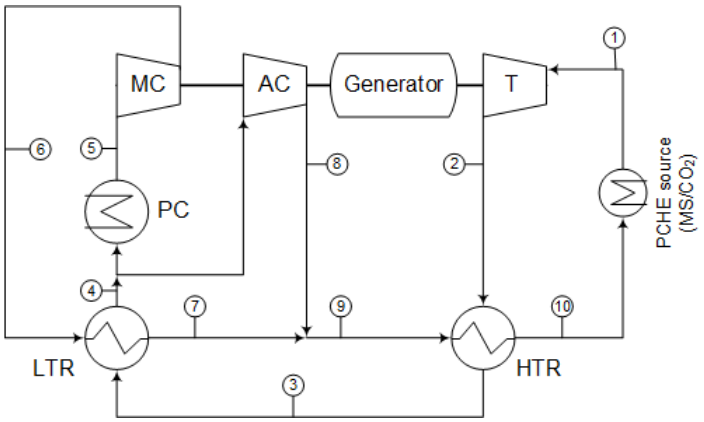

(a) Conventional recompression cycle (RC)

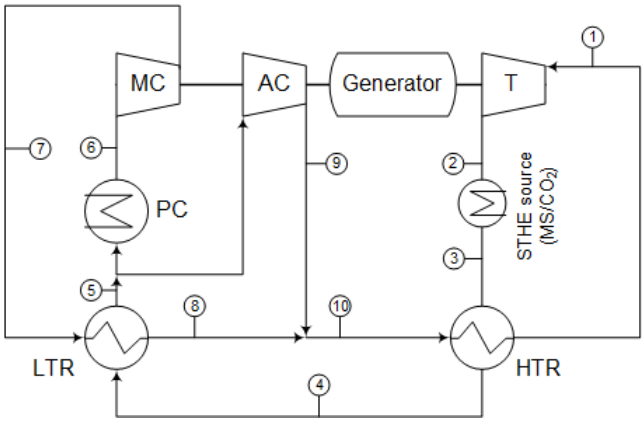

(b) Novel recompression cycle (RC-LP)

Figure 1. Conventional (a) and novel (b) recompression cycle.

The heat power supply through the low pressure side in the proposed cycle is inspired in the so called split expansion cycle [Ahn 2015], although in that case two turbines were used. In the simplest version of such cycle the heat power supply acts as a reheater, that is, supplying the heat power at an intermediate pressure, being the flow downstream the low pressure turbine (LPT), which transfers the heat power to the stream incoming to the high pressure turbine (HPT) in the HTR (Figure 2). In this sense, the proposed layout supresses the low pressure turbine, delivering the heat power in the stream leaving the turbine (the low pressure side) and then transferring it to the stream incoming in the turbine by means of the HTR. Wang et al. [Wang-2017] recommend the split expansion cycle to reduce thermal stress. In the proposed cycle, the reason is similar: reducing the pressure load over the heat exchanger in order to replace the usually required PCHE by a STHE, which allows enough pass area to the molten salt to avoid melting/clogging issues.

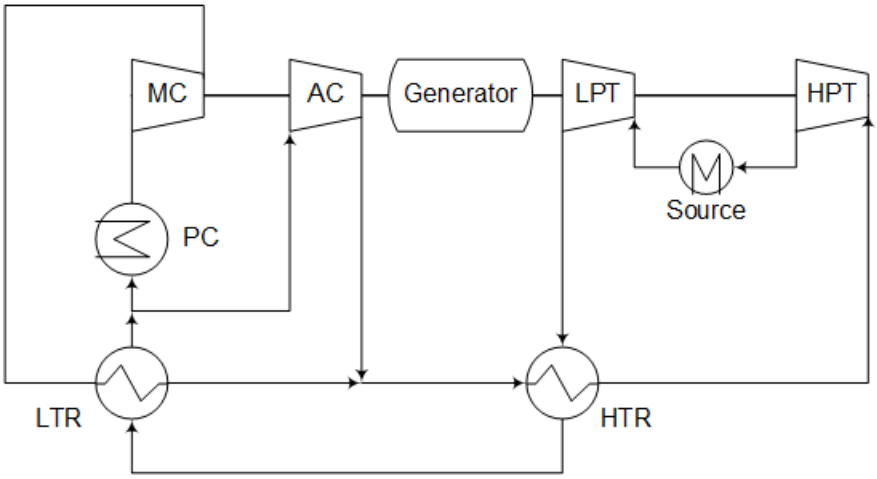

Figure 2. Split expansion layout (adapted from [Wang-2017]).

Four alternatives have been analysed, all of them based on recompression cycle. They include the aforementioned recompression (RC-LP), intercooling (RC-IC-LP), reheating (RC-RH-LP) and intercooling with reheating (RC-IC-RH-LP). Figure 3 shows these layouts.

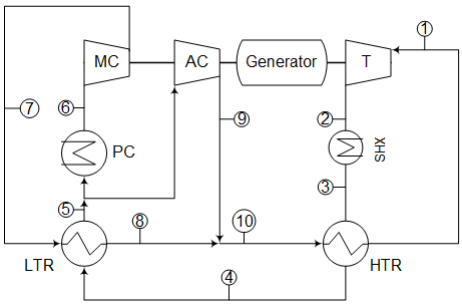

(a) Re-compressed layout (RC-LP).

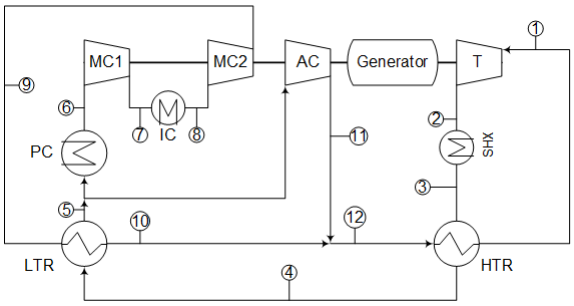

(b) Re-compressed with intercooling (RC-IC-LP).

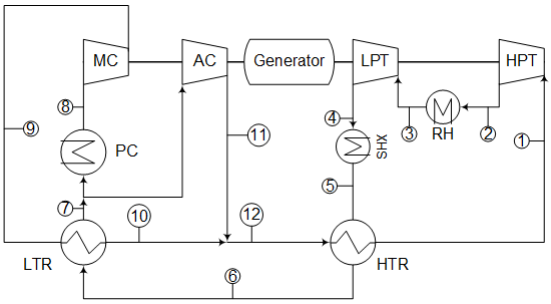

(c) Re-compressed with reheating (RC-RH-LP).

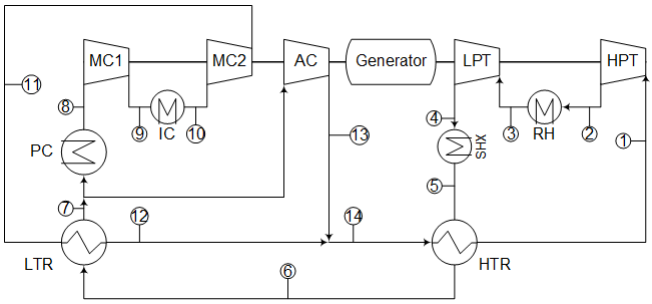

(d) Re-compressed with intercooling and reheating (RC-IC-RH-LP).

Figure 3. Variations of the novel proposed layout.

Main compressor inlet conditions have been taken as 85 bar and 35 °C or 50 °C. The pressure lets reach a reasonable trade-off between closeness to critical point and compressor instability issues, if any [Moisse-2009]. The chosen values for the inlet temperature depend of the cooling system: 35 °C for wet cooling and 50 °C for dry cooling [Ma-2017]. The turbine inlet pressure has been optimised to maximise the cycle

efficiency, being 300 bar the maximum allowed value. The turbine inlet temperature depends of the HTR operation, establishing 688 °C as maximum CO_2 temperature (CO_2 outlet of STHX source heat exchanger). Intercooling and reheating pressures have been also optimised to maximise the cycle efficiency, being the MC2 inlet temperature the same than the MC1 and the LPT inlet temperature the same than the HPT. Isentropic efficiency in compressors has been set at 88% and in turbines at 92%, according to [Bahamonde-2012].

Pressure drop in CO_2 stream into the heat exchangers has been taken as 40 kPa [Medrano-2007]. In the case of molten salt, a maximum velocity of 3 m/s has been selected, according to [CEC-2015]. No pressure drops have been considered in pipes inside the cycle, but an overall value of 5 bar has been assumed in the heat source (molten salt) and heat sink (water in wet cooling case) loops. Minimum approach temperature at PCHEs (LTR, HTR and PC in wet cooling case) has been taken as 5 °C. In the case of STHE heat exchangers an approach of 10-12 °C has been considered.

Three power outputs are defined: cycle, gross and net. Cycle power is the surplus of the turbines regarding the compressors (equation 1); gross power is the result of considering the generator efficiency (η_g), taken as 97% [Lathman] over the cycle power (equation 2) and net power is obtained subtracting the heat source and heat sink loops pumping consumption to the gross power (equation 3). In the case of dry cooling (both pre-cooler and intercooler, if any), 50 kW has been assumed for each electric engine. A cycle power output of 50 MW has been assumed, taking into account the usual values from 10 MWe for first prototypes and 100 MWe for commercial plants [Mehos-2017]. The cycle efficiency takes into account the cycle power and the heat transferred into the cycle by the STHXs (SHX and RH, if any).

$$\dot{W}_{cycle} = \dot{W}_{T,HPT} + \dot{W}_{T,LPT} - \dot{W}_{MC,MC1} - \dot{W}_{MC2} - \dot{W}_{AC} \quad (1)$$

$$\dot{W}_{gross} = \dot{W}_{cycle} \cdot \eta_g \quad (2)$$

$$\dot{W}_{net} = \dot{W}_{gross} - \dot{W}_{HTP} - \dot{W}_{LTP} - \dot{W}_{CP} \quad (3)$$

2.2. Fluid properties

Carbon dioxide, water and air have been modelled as pure substances, using the correlations given at Engineering Equation Solver (EES, [EES]) software. A chloride ternary salt (24.5% NaCl – 20.5% KCl – 55.0% $MgCl_2$, weight composition) has been selected as molten salt due to its allowed operation range (387 °C to more than 800 °C), low volumetric heat capacity ($\rho \cdot c$ = 1.9 J/cm^3-K) and cost (295 $/tonne) [Mohan-2018]. Table 1 gives the properties of the salt.

Table 1. Correlations for property salt.

Property	Correlation	Reference
Specific heat [J/kg-K]	1,180	Mohan, 2018
Density [kg/m^3]	$1{,}899.3 - 0.43 \cdot T$[°C]	Li, 2017
Conductivity [W/m-K]	$0.5423 - 0.0002 \cdot T$[°C]	Li, 2017
Dynamic viscosity [Pa·s]	$8.25 \cdot 10^{-6} \cdot e^{11{,}874.71735/(1{,}350.84595+T[°C])}$	Li, 2017

2.3. Model of heat exchangers

In PCHEs (LTR, HTR in both cooling scenarios and PC in wet cooling scenario), at least one of the streams is CO_2, whose properties are strongly dependent on the temperature and pressure, especially close to the critical point. So, in such heat exchangers an iterative procedure has been implemented dividing the length of the heat exchanger in cells and assuming a continuous variation of the properties [Cantizano-HX]. Specific correlations have been developed for CO_2 heat transfer coefficients, which can be found in [Cabeza – 2017]. For the current analysis, recommendations from Dostal [Dostal-2004] have been followed. PCHEs dimensions have been obtained from Heatric [Le Pierres-2011], taking into account its manufacturing limitations. The manufacturing is modular, being the maximum dimensions of a module (width x length x height) 0.6 m x 0.6 m x 1.5 m, being the height the flow path of the streams. Up to 14 modules can be piled up in parallel in a bonding structure, so constituting the biggest stack. The inner channels are semicircular, with 2 mm diameter and 2.5 mm pitch. Each layer of channels is 1.5 mm width.

Pre-cooler and intercooler in the case of dry cooling are air coolers cross flow heat exchangers. A core sCF-734 has been used, being the air side modelled with the correlations implemented in EES. The air length is controlled to obtain a fan consumption lower than 50 kW. The number of tubes is controlled to obtain a pressure drop lower than 40 kPa. In the CO_2 side, the same discretisation procedure than in the PCHEs has been used, due to the proximity of this stream to the critical point in these heat exchangers.

As stated above, the use of conventional shell and tube heat exchangers is possible thanks to the lower pressure load in the source and the reheater in the novel proposed layout. The primary fluid going through the tubes is CO_2 and the secondary fluid entering in the shell is the ternary chloride molten salt. For the thermofluidynamic model, the heat transfer to the CO_2 in the tubes is calculated by Gnielisnki correlation, and the pressure drop by the Darcy-Weisbach equation [Kakaç-2012]. Averaged CO_2 properties are considered in this case, as the working temperatures are far from the critical point. For the molten salt in the shell, it is suggested to use McAdams correlation to calculate the heat transfer, and the Kern method to determine the pressure drop [Kakaç-2012].

The material used for both the tubes and the shell is a high-nickel alloy, Inconel 625, which is recommended in terms of compatibility and cost [Mehos-2017]. All these STHX have been modelled as counterflow heat exchangers with one shell pass and one tube pass. Regarding the shell type, an "E" shell has been chosen according to Tubular Exchanger Manufacturers Association (TEMA) standards [TEMA-1999]. The minimum tube thickness has been calculated according to ASME (American Society of Mechanical Engineers) Boiling and Pressure Vessel Code [ASME-2019]; based on this lower limit, it has been selected a standardized wall thickness, in terms of the Birmingham Wire Gage (BWG) of the tube. Other manufacturing requirements of this type of heat exchangers have been considered, as the shell-diameter-to-tube-length ratio, which should be within limits of about 1/5 to 1/15. Besides, maximum tube length is limited by architectural layouts and by transportation to about 30 m.

2.4. Heat source and heat sink

2.4.1. Heating and cooling loops

Figure 4 shows both heating and cooling loops. The heating loop includes both source (SHX) and reheating (RH) heat exchangers (if required) of shell and tube type. One pump (HTP) removes the molten salt mass flow rate from the hot tank and another pump (LTP) does the same from the cold pump. A solar multiple of 1.5 has been assumed, so the mass flow rate in the LTP is 1.5 times the one in the HTP. Both pumps are supposed with an efficiency of 75 %. Figure 4 shows the cooling loop in wet cooling scenario. If dry cooling is selected, PC and IC would be air cooled heat exchangers and the fan consumption would come from its electrical engine. An efficiency of 75 % has been assumed for the cooling pump (CP) or the fans (dry cooling). An overall head of 5 bar is assumed for all the pumps. The storage time has been taken as 3 hours, with 6 hours of charge period (both assumed as equivalent at full load). The temperature of the hot tank is 700 °C, depending on the temperature of the cold tank of the power cycle.

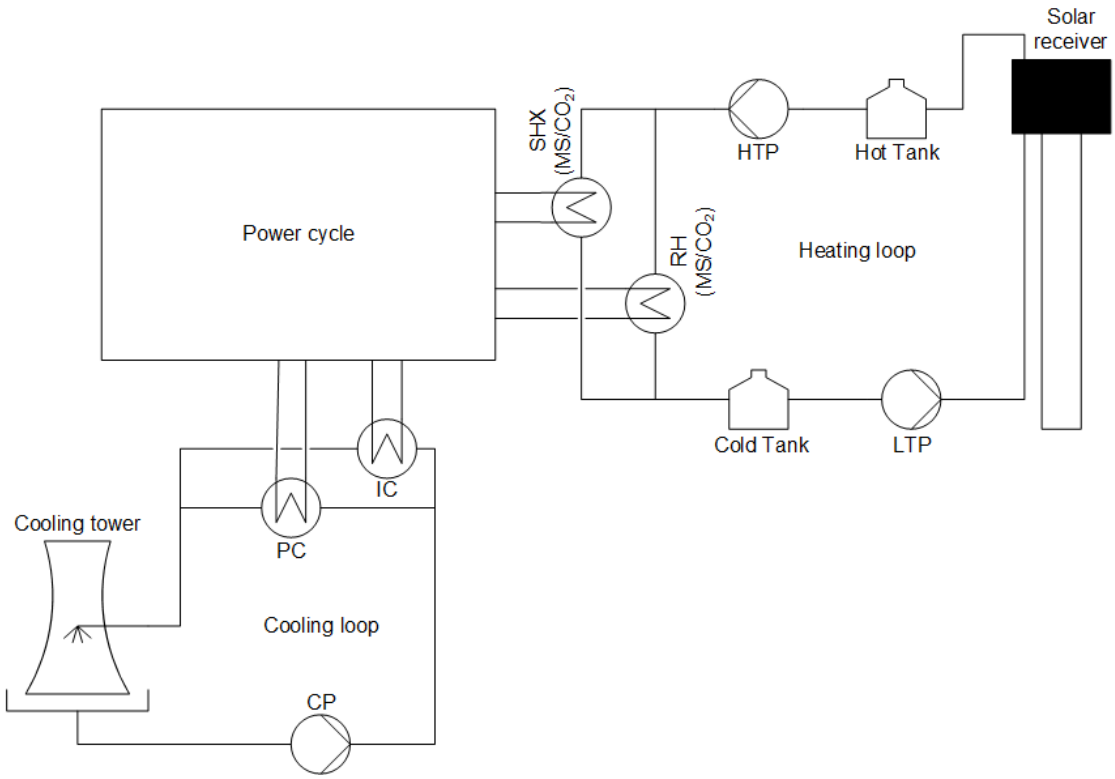

Figure 4. Heating and cooling loops

2.4.2. Receiver and heliostats field

As previously said in the introduction, a tubular cavity-type configuration has been selected for the receiver. As also said before, cavity receivers present lower radiation heat loss and higher convective heat loss than external receivers [Falcone-1986], so they seem to be the best option when working temperature increases and the radiation heat loss becomes critical.

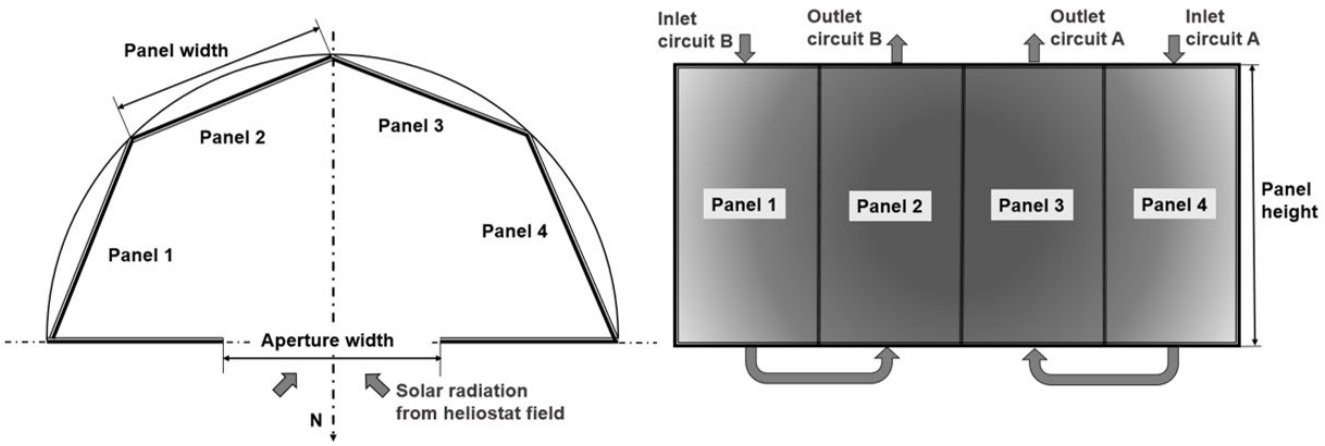

Figure 5. Receiver configuration and fluid flow layout

As seen in Figure 5, the receiver consists of four panels. The fluid flow layout has been divided in two symmetrical circuits. The molten salt goes into the receiver through both side panels of the absorber

surface, the lower temperature zone in the receiver, and then it is circulated to the central panels, to finally leave through the highest temperature region. This flow direction improves the heat transfer, as it reduces the temperature difference between the absorber surface and the molten salt. Other thermal and geometric parameters of the receiver, i.e. the maximum allowable concentrated flux, the tube diameter, the aspect ratio, have been chosen or calculated according to technical literature [Falcone-1986; Zavoico-2001; Liao-2014; Jebamalai-2016].

All receivers have been designed to provide the heat power required for each cycle configuration. For all of them, the average MS velocity inside the tubes has been set to 1.6 m/s, thus ensuring an adequate comparison framework with the same cooling conditions. Since the inlet and outlet MS temperatures are different in each layout, as well as the mass flow, the tube diameters have changed to meet the velocity value requirement.

The thermal model developed for the receiver introduces two main improvements, compared to other models in the literature [Li-2010; Boudaoud-2015]. On one hand, it takes into account the solar and infrared radiosity exchange inside the cavity, applying the semi-gray theory [Siegel-1992]. On the other hand, it calculates the convection heat loss from each of the panels of the receiver, applying the Clausing equation, which gives more accurate results than other more simplified equations [Samanes-2015]. In the end, the receiver performance is higher than that obtained with a simplified model without taking into the cavity effect in a proper way.

For each receiver configuration, it is necessary to calculate the optical efficiency of the associated heliostat field. For this, the program SolarPILOT is used [Wagner-2018]. SolarPILOT is a tool that employs both an analytical flux image Hermite series approximation (based on DELSOL [Kistler-1986]) and a Monte-Carlo ray tracing engine (based on SolTrace [Wendelin-2003]). SolarPILOT offers the possibility of optimizing the optical tower height respect to expected plant productivity over the year. For all the layouts, this optimization yields to a tower height within the recommended values for north-facing fields (Falcone-1986). Besides, SolarPILOT has been integrated into SAM software [Blair-2018], so it also provides an economic assessment of the solar field investment, including the tower and receiver.

2.5. Economic model

The investment cost (fixed capital investment, FCI, according with [Bejan]) has been estimated. This cost include both the direct and indirect costs, taken the latter as 25 % of the former [Bejan], except for the tower, receiver and solar field, as it will be discussed later. Direct costs are divided into on-site costs (ONSC: purchased-equipment costs, installation, piping, instrumentation, controls and electrical equipment) and off-site costs (OFFSC: land, civil works and service facilities). Except when especial scale law is presented,

equation 4 is used to scale the cost, where C_0 stands for the basis cost, C de actual cost, M_0 the basis magnitude, M the actual magnitude and a the escalation factor.

$$C = C_0 \cdot \left(\frac{M}{M_0}\right)^a \quad (4)$$

For the estimation of the power cycle, a study of Sandia National Laboratory [SNL] for a recompression cycle of 10 MWe has been taken as basis. This study allows to convert the purchased-equipment costs (PEC) into on-site costs multiplying by 2.19. The PEC for the main equipment is scaled as follows:

a) PCHEs. The PCHEs are scaled using the number of modules due to the module is the unit of manufacturing. The escalation factor is 0.4 [Bejan], the basis PEC is 5 M$ and the basis number of modules is 4.46 for the HTR and 3 M$ and 3.1, respectively, for the rest of PCHEs. The reason is that the HTR operates at temperatures which demands the use of Inconel 617 alloy, whereas the other heat exchangers are manufactured in SS 316 [Southall-2008].

b) Air cooled heat exchangers. Basis cost is taken as 836,000 $ for a high pressure in SS 316 heat exchanger of inner area (bare tube) of 1,000 m^2 with an escalation factor of 0.526, according with estimation of the engineering company Matches [matches].

c) Turbomachinery and generator. The escalation for the set of main compressor, auxiliary compressor, turbine and generator has been taken from [Driscoll] and is based on the three factors given in equations 5 to 7. Finally, the PEC is given by the equation 8.

$$f_W = \left(\frac{W}{10\ MW}\right)^{0.68} \quad (5)$$

$$f_p = \left(\frac{p}{200\ bar}\right)^{-0.6} \quad (6)$$

$$f_T = \frac{3.35+\left(\frac{T[°C]}{1{,}000}\right)^{7.8}}{3.35+\left(\frac{650\ °C}{1{,}000}\right)^{7.8}} \quad (7)$$

$$PEC_{TMG} = f_W \cdot f_p \cdot f_T \cdot 6\ M\$ \quad (8)$$

Regarding the shell and tube heat exchangers, the PEC has been estimated using the Purohit method [Purohit-1982] that precisely covers this type of heat exchanger and that requires the knowledge of the characteristics, design and operating parameters of the HX. The PEC of the HX is obtained based on the cost estimated for of a baseline heat exchanger corrected by factors that consider the effects of material, pressure and features on costs. The cost, C_E ($), is estimated by the equation (9), supported by the equation (10), where C_b is the cost of the baseline heat exchanger fabricated from base material (carbon steel) ($/ft^2), designed to operate at a given pressure range and for a specific design type (a specific TEMA type, dimensions and geometry),), D_{Sh} is shell inside diameter (in), p is a cost multiplier for tube outside diameter, pitch and layout angle, f is a cost multiplier for TEMA-type front head and r is a cost multiplier for TEMA type rear head; C_i are the factors that correct the base cost due to the differences from the reference heat exchanger [Purohit-1983], and A is the heat transfer area (ft^2). The cost obtained with the

equation (10) is refereed to 1982, so for cost based at different time, an escalation index is applied according with equation (11) where C_{ERy} is the estimated cost at the reference year ($), C_E is the estimated cost at the original year ($) calculated with equation (9), and CI_{Ry}/CI_{Oy} is the ratio of the cost index on the two dates [Vatavuk-2002]. The index used is the Fabricated Equipment component of the Chemical Engineering Plant Cost Index (CEPCI) (reported monthly).

$$C_E = C_b \cdot (1 + \sum_i C_i) \cdot A \quad (9)$$

$$C_b = \left[\frac{6.6}{1-e^{((7-D_{Sh})/27)}}\right] \cdot p \cdot f \cdot r \quad (10)$$

$$C_{ERy} = C_E \cdot \frac{CI_{Ry}}{CI_{Oy}} \quad (11)$$

Cost estimation of the thermal energy storage (TES) system has been taken from the NREL Gen3 roadmap for CSP [Mehos-2017], where the TES with a $MgCl_2$ based salt for 720 °C is taken as basis case. The costs are given as direct costs, so including on-site and off-site ones. The volume of the cold tank is taken as basis magnitude (30,000 m^3), being the escalation factor 0.8. The required salt inventory assumes 10 % of unusable residual at the bottom of the tank for pump suction head. Finally, the volume tank considers 10 % of freeboard above the full-salt level. The basis cost for cold tank is 16.794 M$, for the hot tank 110.119 M$, for structural steel 1.117 M$, for tank insulation 6.6243 M$, for electrical 1.161 M$, for foundations 5.113 M$ and for site work 0.581 M$. The salt inventory cost varies linearly with a specific cost of 295 $/tonne.

The cost of the tower, receiver and heliostats field has been estimated by means of the SolarPILOT software [Wagner-2018]. The on-site cost of the tower is scaled according to equation (12), as a function of the tower height (h_t). The on-site cost of the receiver is scaled with a basis cost of 103 M$, a basis area of 1,571 m^2 and an escalation factor of 0.7. Finally, the on-site heliostats field is scaled linearly with a specific cost of 145 $/$m^2$ of heliostat reflective area. Off-site costs are estimated according with 16 $/$m^2$ for site improvements and 24,710 $/ha for land cost. Specific ratios for contingencies and other indirect costs are implemented in the software.

$$ONSC_{tower}[M\$] = 3 \cdot e^{0.0113 \cdot h_t[m]} \quad (12)$$

3. RESULTS

3.1. Layout selection

Two scenarios have been considered, depending on the heat sink: wet cooling and dry cooling. In the former the main compressor inlet temperature (MCIT) is assumed 35 °C, whereas in the latter 50 °C. In each scenario four layouts have been tested: recompression (RC-LP), recompression with intercooling (RC-IC-LP), recompression with reheating (RC-RH-LP) and finally recompression with intercooling and reheating (RC-IC-RH-LP). When intercooling and/or reheating are used, the intermediate pressure is optimised to maximise the cycle efficiency. In all the cases, the split ratio in the compressors is selected to obtain a balanced LTR. Figures 6 and 7 show the performance of all the layouts in both cooling scenarios, as a function of the turbine inlet pressure (TIP). The cycle efficiency (η) and the CO_2 inlet temperature to the source heat exchanger (SHXIT) are obtained. This temperature is an indicator of the minimum molten salt temperature, which influences in the molten salt inventory, being the maximum temperature given (700 °C).

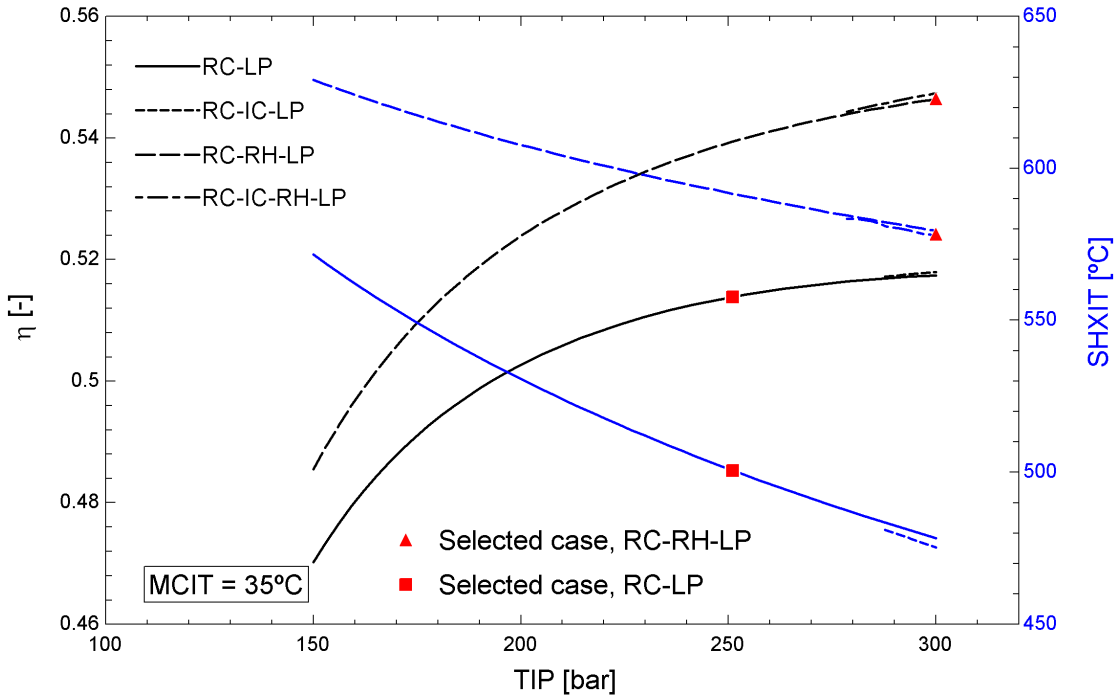

Figure 6. Performances of different layouts when wet cooling is used,

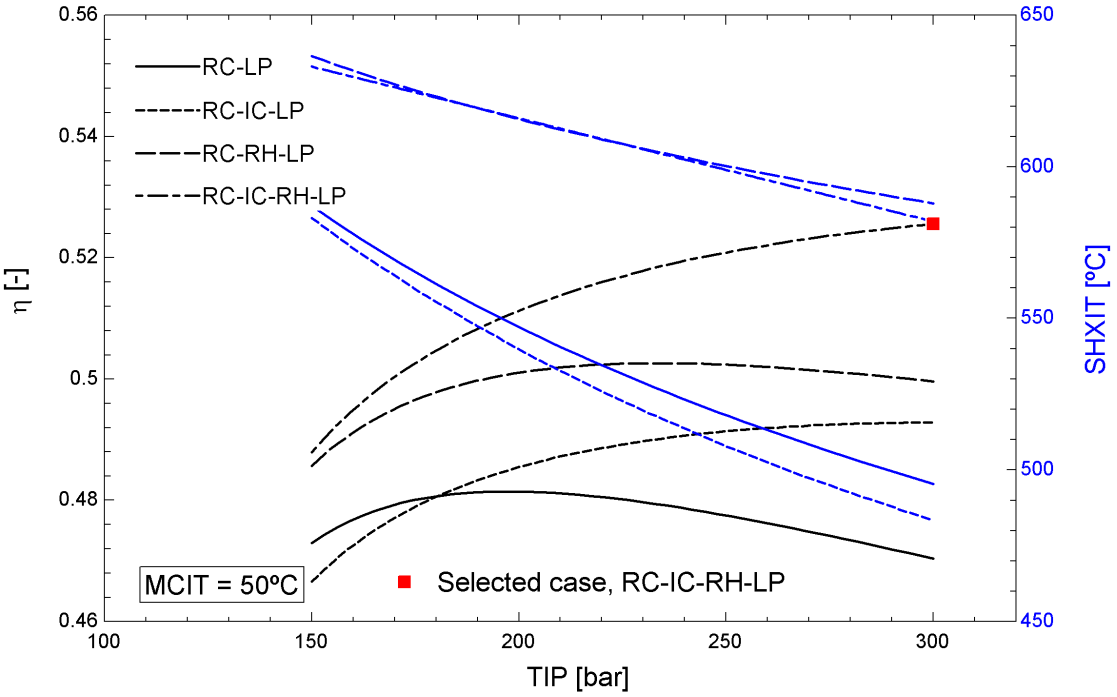

Figure 7. Performances of different layouts when dry cooling is used,

As the main compressor inlet is close to the critical temperature when wet cooling is used, Figure 6 shows no worth is found if intercooling is done (using or not reheating). In fact, only the cases with intercooling pressure higher than 90 bar have been plotted. The situation is clearly different when dry cooling is used, achieving higher efficiencies when intercooling is used, independently of reheating, which is according with [Ma-2017], [Binotti-2017], and [Wang-2018]. In both cooling scenarios the SHXIT increases around 100 °C when reheating is used, independently of intercooling, according with [Wang-2017]. This will lead to a higher cost in TES when reheating is used. Trying to achieve an efficiency higher than 50 %, three cases have been selected, marked with red symbol in Figures 6 and 7. So, when wet cooling is used two configurations have been highlighted: RC-LP at 250 bar and RC-RH-LP at 300 bar. The pressure has been chosen taken into account the sensitivity of the efficiency to the turbine inlet pressure. When dry cooling is used, only the most complex layout (RC-IC-RH-LP) achieves efficiencies well above 50 %. So, 300 bar is selected for this scenario.

Although the feeding in low pressure has been the solution proposed to avoid the melting/clogging issues in the salt, a comparison with the conventional solution is given in Figures 8 and 9. So, Figure 8 compares the selected layouts (recompression and recompression with reheating) in wet cooling scenario, and Figure 9 the recompression with intercooling and reheating when dry cooling is used. When the wet cooling is used the efficiency in the novel cycle is 1.8 percentual points below the conventional case in the recompression layout, but only 0.7 points when reheating is added. Regarding the SHXIT, the behaviour is the opposite: no relevant difference is found when recompression is used, but when reheating is employed,

such temperature increases around 30 °C in the novel cycle. In the case of dry cooling, a low reduction in the efficiency is detected (roughly 0.6 points), being again the SHXIT 24 °C higher.

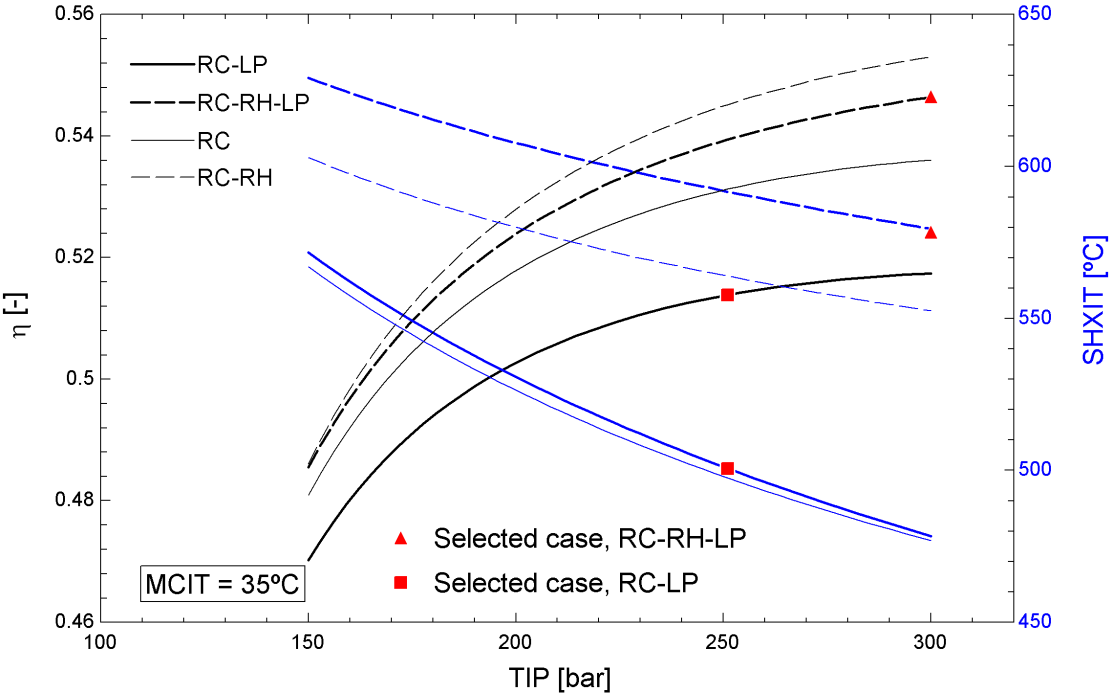

Figure 8. Performance comparison between selected layouts of the novel cycle and the conventional layouts when wet cooling is used.

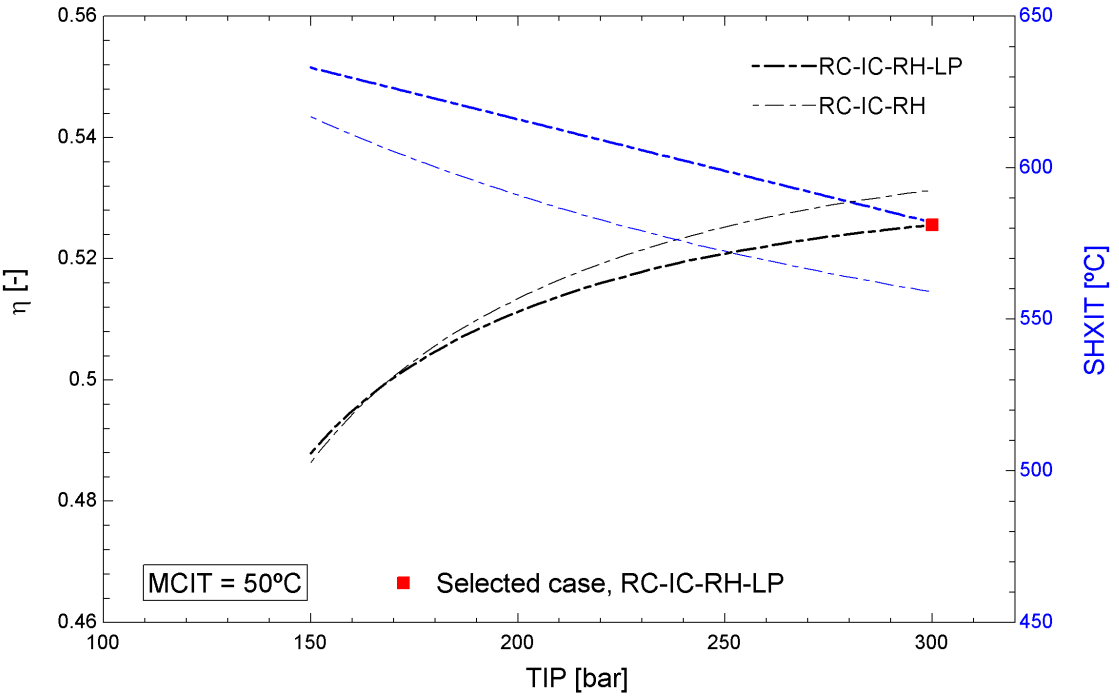

Figure 9. Performance comparison between selected layouts of the novel cycle and the conventional layouts when dry cooling is used.

3.2. Analysis of selected layouts

Figure 10 shows the T-s diagram of the wet cooling scenario and Figure 11 of the dry cooling. Table 2 gives the state points. These Figures and Table are referred to Figure 3 label points. The low pressure heating supply is observed in 2-3 process in Figure 10a and in 4-5 in Figures 10b and 11. In the case of reheating, the intermediate pressure is low enough to allow the use of a STHX heat exchanger, although with large thickness in the tubes.

Table 2. State points of the selected layouts.

	RC-LP (wet cooling)			RC-RH-LP (wet cooling)			RC-IC-RH-LP (dry cooling)		
	p [bar]	T [°C]	h [kJ/kg]	p [bar]	T [°C]	h [kJ/kg]	p [bar]	T [°C]	h [kJ/kg]
1	250	638.6	636.7	300	638.4	634.4	300	645.6	643.6
2	86.6	501.1	478.7	193.4	578.4	564	185.5	579.8	566.3
3	86.2	688	706.4	193	688	701.6	185.1	688	701.9
4	85.8	180.2	107.9	86.6	579.3	572.8	86.6	584.8	579.5
5	85.4	74.6	-29.27	86.2	688	706.4	86.2	688	706.4
6	85	35	-197.9	85.8	208.2	140.2	85.8	236.3	172.2
7	250.8	69.6	-170.7	85.4	81.62	-17.91	85.4	102.4	12.3
8	250.4	175.2	38.19	85	35	-197.9	85	50	-80.9
9	250.4	175.2	38.19	300.8	76.62	-163.2	111.8	71.27	-69.79
10	250.4	175.2	38.19	300.4	203.2	68.19	111.4	50	-155.6
11	---	---	---	300.4	203.2	68.19	300.8	97.43	-120.4
12	---	---	---	300.4	203.2	68.19	300.4	231.3	109.5
13	---	---	---	---	---	---	300.4	231.3	109.5
14	---	---	---	---	---	---	300.4	231.3	109.5

519

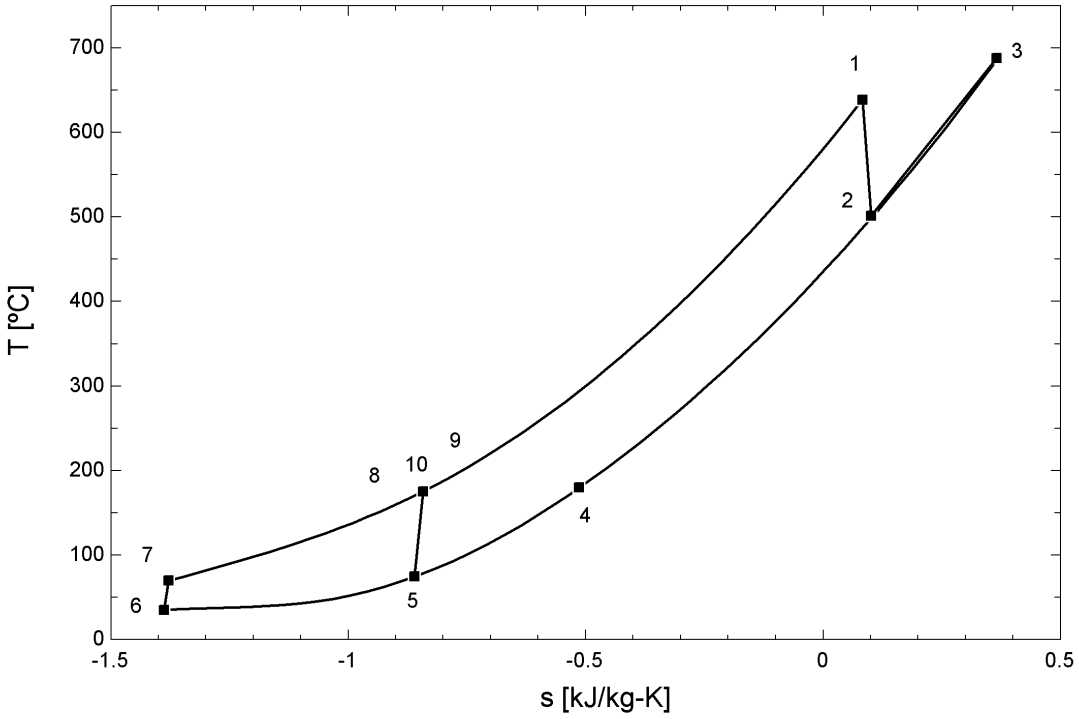

(a) RC-LP

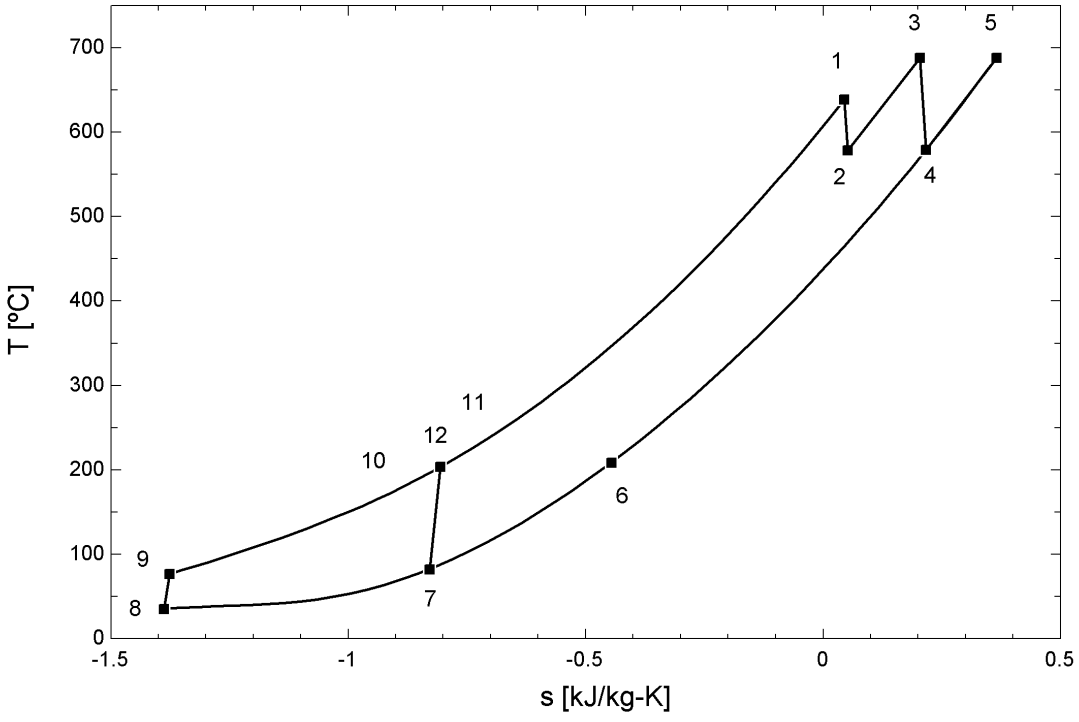

(b) RC-RH-LP

Figure 10. T-s diagrams of the selected layouts when wet cooling is used.

520

521

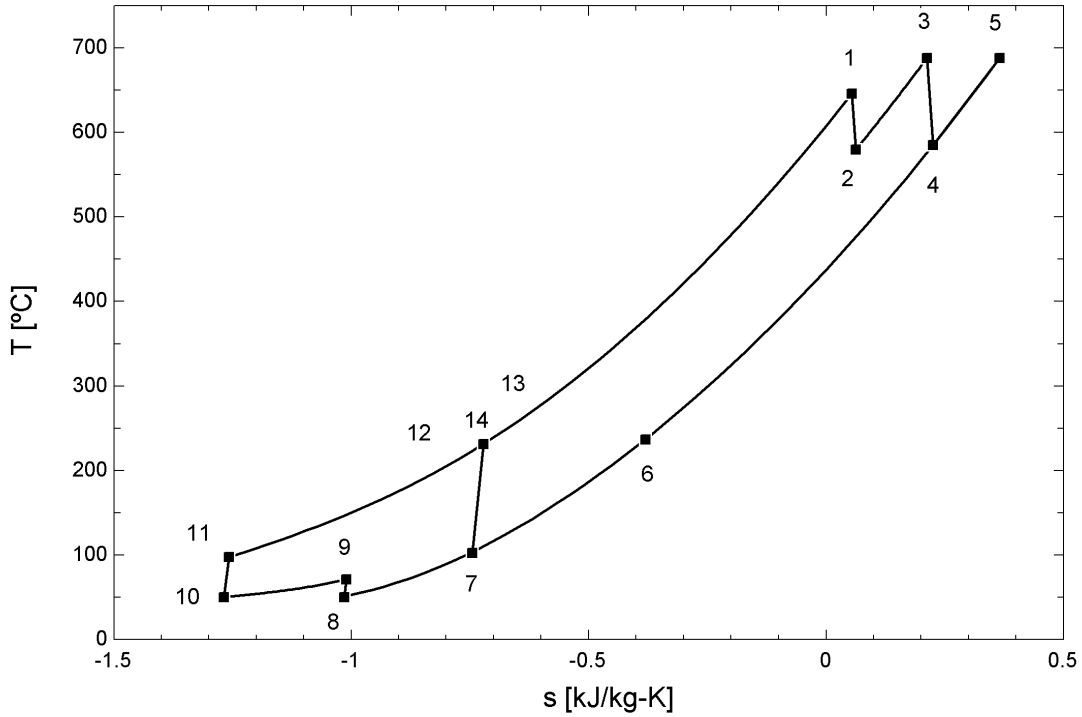

Figure 11. T-s diagram of the selected layout when dry cooling is used (RC-IC-RH-LP)

Table 3 gives the performances of the selected cycles. Table 4 gives the main dimensions of the PCHEs, Table 5 of air cooled heat exchangers and Table 6 of the STHX heat exchangers. Table 7 gives the main characteristics of the storage system: Table 8 gives the main dimensions of the receiver and Table 9 the main dimensions of the heliostats field.

532 Table 3. Performances of the selected layouts (in the case of dry cooling, CP stands for the consumption of the fans).

	Wet cooling		Dry cooling
	RC-LP	RC-RH-LP	RC-IC-RH-LP
MC1 [MW]	7.65	8.00	2.80
MC2 [MW]	---	---	8.87
AC [MW]	9.91	9.2	10.72
HPT [MW]	67.53	23.76	28.04
LPT [MW[	---	43.44	44.36
SHX [MW]	97.33	45.09	45.99
RH [MW]	---	46.42	49.14
PC [MW]	47.33	41.52	23.50
IC [MW]	---	---	21.64
HTP [MW]	0.18	0.22	0.32
LTP [MW]	0.26	0.32	0.47
CP [MW]	0.76	0.67	0.1
$\dot{W}_{cycle}$ [MW]	50.00	50.00	50.00
$\dot{W}_{gross}$ [MW]	48.5	48.5	48.5
$\dot{W}_{net}$ charge period [MW]	47.30	47.29	47.61
$\dot{W}_{net}$ discharge period [MW]	47.56	47.61	48.08
Cycle efficiency [%]	51.37	54.64	52.56

533

534

535

536 Table 4. Main dimensions of PCHEs.

			LTR	HTR	PC
Wet cooling	RC-LP	Heat power [MW]	58.62	255.84	47.33
		Height [m]	3.90	2.66	0.66
		Length [m]	10.74	12.64	3.12
		Width [m]	0.60	0.60	0.60
		Volume [m^3]	25.11	20.17	1.25
		Number of modules	35.80	42.12	5.21
	RC-RH-LP	Heat power [MW]	53.36	191.13	41.52
		Height [m]	4.39	2.62	0.66
		Length [m]	9.36	10.02	2.75
		Width [m]	0.60	0.60	0.60
		Volume [m^3]	24.64	15.72	1.09
		Number of modules	46.80	33.4	4.59
Dry cooling	RC-IC-RH-LP	Heat power [MW]	57.97	193.59	---
		Height [m]	2.82	3.37	---
		Length [m]	11.45	9.35	---
		Width [m]	0.60	0.60	---
		Volume [m^3]	19.36	18.91	---
		Number of modules	38.16	46.74	---

537
538
539
540
541
542
543
544
545
546

Table 5. Main dimensions of air cooled heat exchangers.

			PC	IC
Dry cooling	RC-IC-RH-LP	Heat power [MW]	23.50	21.64
		Tube length [m]	18.2	29.75
		Air length [m]	0.17	0.23
		Frontal area [m^2]	475	510
		Heat transfer inner area [m^2]	3,943	5,899
		Volume [m^3]	78.97	118.1

Table 6. Main dimensions of STHXs.

			SHX	RH
Wet cooling	RC-LP	Number of units	2	---
		Heat power [MW]	48.665	---
		Tube outer diameter [mm]	15.875	---
		Tube thickness [mm]	2.768	---
		Tube pitch [mm]	19.843	---
		Number of tube passes	1	---
		Number of shell passes	1	---
		Heat transfer area [m^2]	17,085	---
		Length [m]	28.36	---
		Shell diameter [m]	2.6	---
	RC-RH-LP	Number of units	1	2
		Heat power [MW]	45.09	23.212
		Tube outer diameter [mm]	19.05	19.05
		Tube thickness [mm]	3.404	5.3
		Tube pitch [mm]	23.81	23.81
		Number of tube passes	1	1.7
		Number of shell passes	1	1
		Heat transfer area [m^2]	12,786	1
		Length [m]	20.43	7,348
		Shell diameter [m]	2.9	15.21
Dry cooling	RC-IC-RH-LP	Number of units	1	2
		Heat power [MW]	45.94	24.57
		Tube outer diameter [mm]	19.05	19.05
		Tube thickness [mm]	3.404	5.3
		Tube pitch [mm]	23.81	23.81
		Number of tube passes	1	1
		Number of shell passes	1	1
		Heat transfer area [m^2]	10,320	8,426
		Length [m]	16.72	15.59
		Shell diameter [m]	2.88	2.69

560 Table 7. Main characteristics of TES.

	Wet cooling		Dry cooling
	RC-LP	RC-RH-LP	RC-IC-RH-LP
Salt inventory [tonnes]	5,157	6,352	9,127
Energy stored [MWh]	292.0	274.6	285.4
Hot tank			
Temperature [°C]	700	700	700
Volume [m^3]	3,549	4,371	6,281
Cold tank			
Temperature [°C]	510	590	595
Volume [m^3]	3,376	4,207	6,109

561

562

563

564 Table 8. Main characteristics of receiver.

	Wet cooling		Dry cooling
	RC-LP	RC-RH-LP	RC-IC-RH-LP
Sizing and geometrical characteristics			
Number of pannels	4	4	4
Pannel width [m]	5.921	5.811	5.945
Pannel height [m]	10.830	10.630	10.875
Aperture width [m]	15.472	15.186	15.535
Aperture height [m]	8.123	7.972	8.156
Number of passes	2	2	2
Inner/outer diameter [mm]	29/32	37/41	50/55
Number of tubes in each pannel	185	141	108
Thermal characteristics			
Thermal power [MWth]	145.995	137.274	142.7055
Solar multiple	1.5	1.5	1.5
Cycle thermal power [MWth]	97.33	91.516	95.137
Inlet MS temperature	510	590	595
Outlet MS temperature	700	700	700
Incident heat [MWth]	152.969	143.964	150.224
Convection heat loss [MWth]	2.017	1.914	1.841
Radiation heat loss [MWth]	5.438	5.384	6.391
Solar radiation heat loss [MWth]	1.050	0.988	1.031
Infrarred radiation heat loss [MWth]	4.388	4.396	5.360
Thermal efficiency	95.126	94.931	94.520
Thermal loss of each pannel			
Convection heat loss [kWth]			
Pannel 1	544.452	508.347	505.307
Pannel 2	463.898	448.611	415.107
Pannel 3	463.898	448.611	415.107
Pannel 4	544.452	508.347	505.307
Solar radiation heat loss [kWth]			
Pannel 1	250.516	235.770	246.022
Pannel 2	274.387	258.235	269.464
Pannel 3	274.387	258.235	269.464
Pannel 4	250.516	235.770	246.022
Infrarred radiation heat loss [kWth]			
Pannel 1	932.228	1000.242	1220.867
Pannel 2	1261.996	1197.848	1459.374
Pannel 3	1261.996	1197.848	1459.374
Pannel 4	932.228	1000.242	1220.867

565

566

567

568 Table 9. Main characteristics of heliostats field.

	Wet cooling		Dry cooling
	RC-LP	RC-RH-LP	RC-IC-RH-LP
Simulated heliostat area [m^2]	216,707	220,893	250,779
Simulated heliostat count	1,501	1,530	1,737
Optimized tower optical height [m]	112.977	109	113.655
Cloudiness efficiency [%] min/mean/max	100/100/100	100/100/100	100/100/100
Shading efficiency [%] min/mean/max	100/100/100	100/100/100	100/100/100
Cosine efficiency [%] min/mean/max	62.35/80.77/93.37	62.23/80.55/93.23	61.93/80.4/93.29
Reflection efficiency [%] min/mean/max	90.25/90.25/90.25	90.25/90.25/90.25	90.25/90.25/90.25
Blocking efficiency [%] min/mean/max	55.59/97.03/100	57.34/97.22/100	55.83/96.24/100
Attenuation efficiency [%] min/mean/max	90.45/93.35/97.03	90.18/93.24/97.07	89.63/92.83/97.02
Image intercept efficiency [%] min/mean/max	5.13/72.01/97.55	5.79/70.18/97.01	3.66/68.44/97.69
Solar field optical efficiency [%] min/mean/max	2.63/47.54/78.69	2.95/46.77/77.94	1.55/45.06/79.08

569

570

3.3. Investment estimation

Tables 10 and 11 summarise the investment in the wet cooling scenario and Table 12 in the dry cooling. The fixed capital investment in wet cooling scenario ranges from 456.1 M$ for recompression layout to 464.8 M$ for recompression with reheating; in dry cooling the fixed capital investment is 469.0 M$. These values lead to 9,123 $/kWe in recompression and 9,296 $/kWe in recompression with reheating, both in wet cooling scenario, and 9,381 $/kWe in dry cooling one. Projections of the Gen3 Roadmap [Mehos-2017] establish 200 M$ for a prototype of 10 MWe. Scaling to 50 MWe it would became into 579 M$. In such projections, a TES of 1,350 MWh-th for 50 MWe is considered, with a cost (direct plus indirect) of 112.6 M$. Subtracting this cost to the projected investment and adding the cost of the TES in the proposed layuouts (from 32.6 to 52.1 M$, considering both direct and indirect costs) results a range for the investment between 499.0 to 518.5 M$. So, the proposed layout reduces the projections of Gen3 Roadmap between 8.6 to 9.5%. Taking into account the uncertainties in the economic model, it would be better of saying that the proposed layout investment is according with the Gen3 Roadmap forecasts.

Figure 12 shows an investment breakdown of the selected options into the main components. The heat exchangers contribution rounds 50%, being followed by the solar field, tower and receiver, which accumulates 35%. The turbomachines contribution is similar in all the cases (10%), ranging the storage system share from 7% in RC-LP wet cooling to 11% in RC-IC-RH-LP dry cooling. The cost increase of the storage system is due to the molten salt cold temperature reduction in the reheated layouts (85 °C in RC-IC-RH-LP regarding to RC-LP), which leads to an increase of 77% in the salt inventory.

Table 10. Summary of investments in RC-LP (wet cooling scenario).

	PEC [M$]	Direct costs [M$]		Indirect costs [M$]
		ONSC [M$]	OFFSC [M$]	
Turbomachinery	15.8	34.4	---	60.5
PCHEs				
LTR	8.0	17.4	---	
HTR	12.3	26.8	---	
PC	3.7	8.0	---	
Air Cooled heat exchangers				
PC	---	---	---	
IC	---	---	---	
STHXs				
SHX (two units; total cost)	59.3	129.2	---	
RH	---	---	---	
TES	---	26.1		
Tower	---	10.8	---	10.9
Receiver	---	91.3	---	
Solar Field	---	31.4	---	
Lands, site improvements	---	---	9.3	
Fixed capital investment [M$]		456.1		

598 Table 11. Summary of investments in RC-RH-LP (wet cooling scenario).

	PEC [M$]	Direct costs [M$]		Indirect costs [M$]
		ONSC [M$]	OFFSC [M$]	
Turbomachinery	14.1	30.8	---	62.2
PCHEs				
LTR	8.9	19.4	---	
HTR	11.2	24.4	---	
PC	3.5	7.6	---	
Air Cooled heat exchangers				
PC	---	---	---	
IC	---	---	---	
STHXs				
SHX	25.9	56.4	---	
RH	36.3	79.2	---	
TES	---	31.0		
Tower	---	10.28	---	11.22
Receiver	---	91.1	---	
Solar Field	---	32.029	---	
Lands, site improvements	---	---	9.3	
Fixed capital investment [M$]		464.8		

599

600

601 Table 12. Summary of investments in RC-IC-RH-LP (dry cooling scenario).

	PEC [M$]	Direct costs [M$]		Indirect costs [M$]
		ONSC [M$]	OFFSC [M$]	
Turbomachinery	14.1	30.8	---	61.7
PCHEs				
LTR	8.9	19.4	---	
HTR	11.8	25.7	---	
PC	---	---	---	
Air Cooled heat exchangers				
PC	1.72	3.75	---	
IC	2.13	4.64	---	
STHXs				
SHX	19.7	43.0	---	
RH (2two units; total cost)	35.7	77.9	---	
TES	---	41.7		
Tower	---	10.8	---	12.2
Receiver	---	91.4	---	
Solar Field	---	36.4	---	
Lands, site improvements	---	---	9.7	
Fixed capital investment [M$]		469.0		

602

603

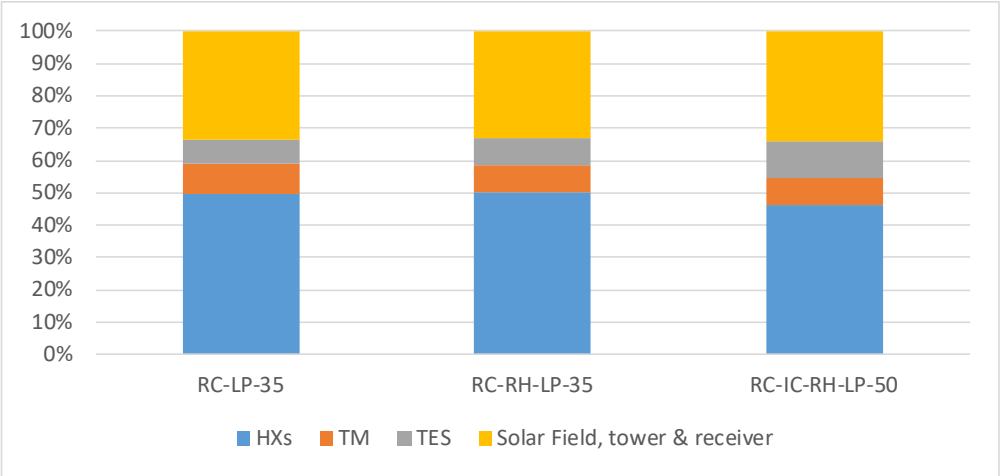

604

605 Figure 12. Investment (fixed capital investment) breakdown of the selected options.

606

607

4. CONCLUSIONS

A novel supercritical CO_2 Brayton power cycle has been proposed for power tower concentrating solar plants. The cycle faces the melting/clogging issues warned by several researches when molten salt circulates along the narrow channels of printed circuit heat exchangers, required to support the high pressures of the conventional supercritical CO_2 Brayton cycle. To deal with these concerns the novel cycle supplies the heat power through the low pressure side (85 bar for the main heat input and less than 200 bar for the reheating input), so allowing the replacement of printed circuit heat exchangers by shell and tubes ones, circulating the molten salt across the shell. Technical and economic assessments of the novel cycle have been carried out.

Two scenarios have been investigated: dry cooling and wet cooling. In the former, the highest efficiency layout is recompression with intercooling and reheating, reaching 52.6 % efficiency at 300 bar of turbine inlet pressure. Options without reheating (with or without intercooling) have been discarded because they do not reach 50 %, while reheating with intercooling does it at 225 bar. In the wet cooling scenario, the recompression cycle (neither intercooled not reheated) exceeds 51 % efficiency at 250 bar, climbing up to more than 54 % if reheating in added. The efficiency does not take advantage of intercooling in wet scenario. If 50 % cycle efficiency is set as a goal for advanced solar plants, recompression in wet cooling scenario might be a first prototype to test this new technology, loosing 1.8 percentual points regarding the conventional supercritical CO_2 Brayton cycle (with the concerns in printed circuit heat exchangers). The inclusion of reheating always reduces the molten salt temperature gap, so increasing the salt inventory (nearly 24 % in wet scenario).

Regarding the economic assessment, all the analysed layouts ranges between 9,123 to 9,381 $/kWe for a plant of 50 MWe, according with the projections of Gen3 Roadmap.

5. AKNOWLEDGEMENTS

This work has been developed in the frame of the ACES2030-CM project, funded by the Regional Research and Development in Technology Programme 2018 (ref. P2018/EMT-4319).

6. REFERENCES

[Mehos-2017] M. Mehos, C. Turchi, J. Vidal, M. Wagner, Z. Ma, C. Ho, W. Kolb, C. Andraka, A. Kruizenga, Concentrating Solar Power Gen3 Demonstration Roadmap, NREL, NREL/TP-5500-67464, 2017.

[ASTRI] H. Gurgenci, W. Stein, A. Beath, M. Blanco, E. Sauret, The case for supercritical CO_2 radial turbine development within the Australian Solar Thermal Research nitiative (ASTRI) program, Proceedings of the 52nd Annual Conference, Australian Solar Energy Society (Australian Solar Council), Melbourne, May 2014.

[Zhang-2018] J. Zhang, Dynamic modelling and transient analysis of a molten salt heated recompression supercritical CO_2 Brayton cycle, Proceedings of the 5th International Supercritical CO_2 Power Cycles Symposium, Pennsylvania, USA, March 2018.

[Myers-2016] P.D. Myers, D.Y. Goswami, Thermal energy storage using chloride salts and their eutectics, Applied Thermal Engineering 109 (2016) 889-900.

[Li-2017] Y. Li, X. Xu, X. Wang, P. Li, Q. Hao, B. Xiao, Survey and evaluation of equations for thermophysical properties of binary/ternary eutectic salts from NaCl, KCl, $MgCl_2$, $CaCl_2$ and $ZnCl_2$ for heat transfer and thermal storage fluids in CSP, Solar Energy 152 (2017) 57-79.

[Mohan-2018] G. Mohan, M. Venkataraman, J. Gomez-Vidal, J. Coventry, Assessment of a novel ternary eutectic chloride salt for next generation high-temperature sensible heat storage, Energy Conversion and Management 167 (2018) 156-164.

[Xu-2018] X. Xu, G. Dehghani, J. Ning, P. Li, Basic properties of eutectic chloride salts NaCl-KCl-$ZnCl_2$ and NaCl-KCl-$MgCl_2$ as HTFs and thermal storage media measured using simultaneous DSC-TGA, Solar Energy 162 (2018) 431-441.

[Turchi-2019] C. S. Turchi, J. Vidal, M. Bauer, Molten salt power towers operating at 600–650 °C: Salt selection and cost benefits, Solar Energy 164 (2018) 38–46.

[Ho, 2014] C.K. Ho, B.D. Iverson, Review of high-temperature central receiver designs for concentrating solar power, Renewable and Sustainable Energy Reviews, 29 (2014), 835-846

[Saravanamuttoo] H.I.H. Saravanamuttoo, G.F.C. Rogers, H. Cohen, P.V. Straznicky, A.C. Nix, Gas Turbine Theory, Pearson, 7th edition, 2017.

[Herranz-2009] L.E. Herranz, J.I. Linares, B.Y. Moratilla, Power cycle assessment of nuclear high temperature gas-cooled reactors, Applied Thermal Engineering 29 (2009) 1759-1765.

[Pérez-Pichel-2011] G. Pérez-Pichel, J.I. Linares, L.E. Herranz, B.Y. Moratilla, Potential application of Rankine and He-Brayton cycles to sodium fast reactors, Nuclear Engineering and Design 241 (2011) 2643-2652.

673 [Pérez-Pichel-2012] G. Pérez-Pichel, J.I. Linares, L.E. Herranz, B.Y. Moratilla, Thermal analysis of
674 supercritical CO_2 power cycles: assessment of their suitability to the forthcoming
675 sodium fast reactors, Nuclear Engineering and Design 250 (2012) 23-34.
676 [Sulzer-1950] G. Sulzer, Verfahren zur Erzeugung von Arbeit aus Warme, Swiss Patent 269599,
677 1950.
678 [Angelino-1968] G. Angelino, Carbon dioxide condensation cycles for power production, Journal of
679 Engineering Power 90 (1968) 287–295.
680 [Feher-1968] E.G. Feher, The supercritical thermodynamic power cycle, Energy Conversion 8
681 (1968) 85–90.
682 [Dostal-2004] V. Dostal, A Supercritical Carbon Dioxide Cycle for Next Generation Nuclear
683 Reactors, Institute of Technology, Massachusetts, 2004 Feb. Doctoral Thesis.
684 [Wang-2017] K. Wang, Y.L. He, H.H. Zhu, Integration between supercritical CO_2 Brayton cycles and
685 molten salt solar power towers: A review and comprehensive comparison of
686 different cycle layouts, Applied Energy 195 (2017) 819-836.
687 [Ma-2017] Y. Ma, M. Liu, J. Yan, J. Liu, Thermodynamic study of main compression intercooling
688 effects on supercritical CO_2 recompression Brayton cycle, Energy 140 (2017) 746-
689 756.
690 [Binotti-2017] M. Binotti, M. Astolfi, S. Campanari, G. Manzolini, P. Silva, Preliminary assessment of
691 SOC2 cycles for power generation in CSP solar tower plants, Applied Energy 204
692 (2017) 1007-1017.
693 [Iverson-2013] B.D. Iverson, T.M. Conboy, J.J. Pasch, A.M. Kruizenga, Supercritical CO_2 Brayton cycles
694 for solar-thermal energy, Applied Energy 111 (2013) 957-970
695 [Ahn-2015] Y. Ahn, S.J. Bae, M. Kim, S.K. Cho, S. Baik, J.I. Lee, J.E. Cha, Review of supercritical CO_2
696 power cycle technology and current status of research and development, Nuclear
697 Engineering Technology 47 (2015) 647–661.
698 [Li-2017-2] M. Li, H. Zhu, J. Guo, K. Wang, W. Tao, The development technology and applications
699 of supercritical CO_2 power cycle in nuclear energy, solar energy and other energy
700 industries, Applied Thermal Engineering 126 (2017) 255–275.
701 [Turchi-2013] C.S. Turchi, Z. Ma, T.W. Neises, M.J. Wagner, Thermodynamic study of advanced
702 supercritical carbon dioxide power cycles for concentrating solar power systems,
703 Journal of Solar Energy Engineering 135 (2013) 041007-1; 041007-7.
704 [Milani-2017] D. Milani, M.T. Luu, R. McNaughton, A. Abbas, Optimizing an advanced hybrid of
705 solar-assisted supercritical CO_2 Brayton cycle: a vital transition for low-carbon
706 power generation industry, Energy Conversion and Management 148 (2017) 1317–
707 1333.

[Wang-2018] K. Wang, M.J. Li, J.Q. Guo, P. Li, Z.B. Liu, A systematic comparison of different S-CO_2 Brayton cycle layouts based on multi-objective optimization for applications in solar power tower plants, Applied Energy 212 (2018) 109-121.

[Xu-2019] J. Xu, Ch. Liu, E. Sun, J. Xie, M. Li, Y. Yang, J. Liu, Perspective of S-CO_2 power cycles, Energy 186 (2019) 115831.

[Ma-2011] Z. Ma, C.S. Turchi, Advanced Supercritical Carbon Dioxide Power Cycle Configurations for Use in Concentrating Sola Power Systems, Proceedings of the 3rd Supercritical CO_2 Power Cycle Symposium, Colorado, USA, May 2011.

[Le Pierres-2011] R.L. Pierres, D. Southall, S. Osborne, Impact of Mechanical Design Issues on Printed Circuit Heat Exchangers, Proceedings of 3rd SCO2 Power Cycle Symposium, Colorado, USA, May 2011.

[Southall-2008] D. Southall, R.L. Pierres, S.J. Dewson, Design considerations for compact heat exchangers, Proceedings of ICAPP '08, California, USA, June 2008.

[Huang-2019] Ch. Huang, W. Cai, Y., Wang, Y. Liu, Q. Li, B. Li, Review on the characteristics of flow and heat transfer in printed circuit heat exchangers, Applied Thermal Engineering 153 (2019) 190-205.

[Moore-2010] R. Moore, M. Vernon, C.K. Ho, N.P. Siegel, G.J. Kolb, Design Considerations for Concentrating Solar Power Tower Systems Employing Molten Salt, Sandia Report SAND2010-6978, 2010.

[Sabharwall-2014] P. Sabharwall, D. Clark, M. Glazoff, G. Zheng, K. Sridharan, M. Anderson, Advanced heat exchangers development for molten salts, Nuclear Engineering and Design 280 (2014) 42-56.

[Lao-2019] J. Lao, J. Ding, Q. Fu, W. Wang, J. Lu, Heat Transfer between Molten Salt and Supercritical CO_2 in Discontinuous Fins Print Circuit Heat Exchanger, Energy Procedia 158 (2019) 5832-5837.

[Wang-2019] W.Q. Wang, Y. Qiu, Y.L. He, H.Y. Shi, Experimental study on the heat transfer performance of a molten-salt printed circuit heat exchanger with airfoil fins for concentrating solar power, International Journal of Heat and Mass Transfer 135 (2019) 837-846.

[Kruizenga-2014] A. Kruizenga, D. Fleming, Materials Corrosion Concerns for Supercritical Carbon Dioxide Heat Exchangers, Sandia National Laboratories, SAND2014-15095PE, 2014.

[He-2016] Y.L. He, Z.J. Zheng, B.C. Du, K. Wang, Y. Qiu, Experimental investigations on turbulent heat transfer characteristics of molten salt in a shell-and-tube heat exchanger, Applied Thermal Engineering 108 (2016) 1206-1213.

[Qiu-2018] Y. Qiu, M.J. Li, W.Q. Wang, B.C. Du, K. Wang, An experimental study on the heat transfer performance of a prototype molten-salt rod baffle heat exchanger for concentrated solar power, Energy 156 (2018) 63-72.

[EFDA 2013] J.I. Linares, L.E. Herranz, I. Fernández-Berceruelo, B.Y. Moratilla, A. Cantizano,Design, modelling and analysis of primary heat transfer and BoP options for integration with a DEMO fusion power plant: FINAL REPORT on supercritical CO_2 Brayton power cycles. Report for Task Agreement WP13-DAS08-T02-BOP (EFDA_D_2L58SM, https://user.efda.org/?uid=EFDA_D_2L58SM) 2013.

[Linares EFDA] J.I. Linares, A. Cantizano, E. Arenas, B.Y. Moratilla, V. Martín-Palacios, Ll. Batet, Recupefated versus single-recuperator re-compressed supercritical CO_2 Brayton power cycles for DEMO fusion reactor based on dual coolant lithium lead blanket, Energy 140 (2017) 307-317.

[Moisse-2009] A. Moisseytsev, J.J. Sienicki, Investigation of alternative layouts for the supercritical carbon dioxide Brayton cycle for a sodium-cooled fast reactor, Nuclear Engineerning and Design, 239 (2009) 1362-1371.

[Bahamonde-2012] J.S. Bahamonde-Noriega, Design Method for S-CO2 Gas Turbine Power Plants, Delft University of Technology, The Netherlands, 2012 (MSc Dissertation).

[Medrano-2007] M. Medrano, D. Puente, E. Arenaza, B. Herrazti, A. Paule, B. Brañas, A. Orden, M. Domínguez, R. Stainsby, D. Maisonnier, P. Sardain, Power conversion cycles study for He-cooled reactor concepts for DEMO, Fusion Engineering and Design (2007) 2689-2695.

[CEC-2015] M. Jonemann, H. Russell, R. Blair, J. Raade, C. Ames, System integration of containerized molten salt thermal energy storage in novel cascade layout". California Energy Commission. Energy Research and Development Division. (CEC-500-2016-006), 2015

[Latham] H. Latham, P. Clarkson, Fusion Balance of Plant Assessment (under EFDA Work Package WP12-DAS08-BoP, IDM reference No. 2LLNBX, 2013).

[EES] S.A. Klein, G.F. Nellis, Mastering EES, F-Chart Software, edition 63 (http://www.fchartsoftware.com/ees/mastering-ees.php)

[Cantizano-HX] I.P. Serrano, A. Cantizano, J.I. Linares 89, B.Y. Moratilla, Modeling and sizing of he heat exchangers of a new supercritical CO_2 Brayton power cycle for energy conversion for fusion reactors, Fusion Engineering and Design 89 (2014) 1905-1908.

[Cabeza-2017] Supercritical CO_2 as heat trasnfer fluid: A review, Applied Thermal Engineering 125 (2017) 799-810.

[Kakaç-2012] S. Kakaç, H. Liu and A. Pramuanjaroenkij, Heat Exchangers: Selection, Rating, and Thermal Design, Ed. Taylor & Francis. Third Edition (2012). ISBN: 978-1- 4398-4990-3

[TEMA-1999] Standards of the Tubular Exchanger Manufacturers Association, TEMA (Tubular Exchanger Manufacturers Association), Tarrytown, NY, 8th edition, 1999

[ASME-2019] ASME Boiling and Pressure Vessel Code, 2019.

[Falcone-1986] P.K. Falcone, A Handbook for Solar Central Receiver Design, SAND 86-8009 (1986)

[Zavoico-2001] A.B. Zavoico, Solar Power Tower. Design Basis Document, Sandia Report SAND2001-2100, 2001.

[Liao-2014] Z. Liao, X. Li, C. Xu, C. Chang, Z. Wang, Allowable flux density on a solar central receiver, Renewable Energy 62 (2014) 747-753

[Jebamalai-2016] J. S. M. Jebamalai, Receiver Design Methodology for Solar Tower Power Plants, Master Thesis, Department of Energy Technology, KTH Industrial Engineering and Management (2016).

[Li-2010] X. Li, W. Kong, Z. Wang, C. Chang, F. Bai, Thermal model and thermodynamic performance of molten salt cavity receiver, Renewable Energy 35 (2010) 981–988.

[Boudaoud-2015] S. Boudaoud, A. Khellaf, K. Mohammedi, O. Behar, Thermal performance prediction and sensitivity analysis for future deployment of molten salt cavity receiver solar power plants in Algeria, Energy Conversion and Management 89 (2015) 655–664.

[Siegel-1992] R. Siegel, J.R. Howell, Thermal Radiation Heat Transfer, Ed. Taylor & Francis. Third Edition (1992). ISBN: 0-89116-271-2

[Samanes-2015] J. Samanes, J. García-Barberena, F. Zaversky, Modeling solar cavity receivers: a review and comparison of natural convection heat loss correlations, Energy Procedia 69 (2015) 543 – 552

[Wagner-2018] M. J. Wagner, T. Wendelin, SolarPILOT: A power tower solar field layout and characterization tool, Solar Energy 171 (2018) 185–196.

[Kistler-1986] B. Kistler, A user's Manual for DELSOL3: A Computer Code for Calculating the Optical Performance and Optimal System Design for Solar Thermal Central Receiver Plants., Sandia Report SAND86-8018 (1986).

[Wendelin-2003] T. Wendelin, SolTRACE: a new optical modeling tool for concentrating solar optics. In: ASME 2003 International Solar Energy Conference, Kohala Coast, HI (2003)

[Blair, 2018] N. Blair, N. Diorio, J. Freeman, P. Gilman, S. Janzou, T. Neises, M. Wagner, System Advisor Model (SAM) General Description System Advisor Model. Tech. Rep. NREL/TP-6A20-70414 (2018).

[Bejan] A. Bejan, G. Tsatsaronis, M. Moran, Thermal Design & Optimization, Wiley, 1996

[SNL] D.D. Fleming et al., Scaling Considerations for a Multi-Megawatt Class Supercritical CO_2 Brayton Cycle and Commercialization, SANDIA REPORT SAND2013-9106 (2013).

[matches] https://www.matche.com/equipcost/Exchanger.html

[Driscoll-2004] M.J. Driscoll, P. Hejzlar, 300 MWe Supercritical CO_2 Plant Layout and Design, MIT Nuclear Engineering Department (2004), MIT-GFR-014

[Purohit-1983] G.P. Purohit, Estimating costs of shell-and-tube heat exchangers, Chemical Engineering 22 (1983) 56-67.

[Vatavuk 2002] W.M. Vatavuk, Updating the CE Plant Cost index, Chemical Engineering 109 (2002) 62-70.

[Wagner-2018] M.J. Wagner, SolarPILOT. Software version 1.3.8 (2018), National Renewable Energy Laboratory (NREL), Golden, Colorado, USA (https://www.nrel.gov/csp/solarpilot.html)